ORNL/CP-99522

INTERFACIAL DEBONDING VERSUS FIBER FRACTURE IN FIBER-REINFORCED CERAMIC COMPOSITES

Chun-Hway Hsueh,[a] Ming-Yuan He,[b] and Paul F. Becher[a]

[a]Metals and Ceramics Division, Oak Ridge National Laboratory, Oak Ridge, TN 37831, USA.

[b]Materials Department, University of California, Santa Barbara, CA 93106, USA.

Toughening of fiber-reinforced ceramic composites by fiber pullout relies on debonding at the fiber/matrix interface prior to fiber fracture when composites are subjected to tensile loading. The criterion of interfacial debonding versus crack penetration has been analyzed for two semi-infinite elastic plates bonded at their interface. When a crack reaches the interface, the crack either deflects along the interface or penetrates into the next layer depending upon the ratio of the energy release rate for debonding versus that for crack penetration. This criterion has been used extensively to predict interfacial debonding versus fiber fracture for a crack propagating in a fiber-reinforced ceramic composite. Two modifications were considered in the present study to address the debonding/fracture problem. First, we derived the analysis for a strip of fiber, which had a finite width and was sandwiched between two semi-infinite plates of matrix. It was found that the criterion of interfacial debonding versus fiber fracture depended on the fiber width. Second, a bridging fiber behind the crack tip was considered where the crack tip initially circumvented the fiber. Subsequent to this, either the interface debonded or the fiber fractured. In this case, we have considered a bridging-fiber geometry to establish a new criterion.

1. INTRODUCTION

The tendency of a wedge-loaded crack meeting a bimaterial interface to either deflect into the interface or penetrate through the interface into the next layer has been analyzed earlier [1]. The analysis was conducted in terms of the energy release rate ratio of crack deflecting into the interface, G_d, to crack penetrating the interface, G_p. The criterion of deflection versus penetration was then established depending on whether G_d/G_p was greater or less than the fracture energy ratio of the interface Γ_i to the adjoining layer, Γ_f. This criterion has been adopted extensively to predict interfacial debonding versus reinforcement fracture for fiber- (whisker- and self-) reinforced ceramic composites. However, due to the assumptions made in the asymptotic analysis [1], in which integral equation methods were used, two limitations should be noted before the criterion is applied. First, the results were obtained based on the condition that the branch crack (i.e., the branched section of the crack emanating from the main crack) was very small compared with all other lengths in the problem. Second, the analysis was for two semi-infinite elastic materials bonded at the interface. For the two-dimensional crack initiation problem, the branch crack can be treated as an infinitely small crack; therefore, these two assumptions are satisfied. However, in some cases (e.g., for a wedge-loaded crack [2,3], or in the presence of residual stress), the length of the branch crack and the width of reinforcement become important, and these two conditions are not satisfied. Also, the crack propagation problem in fiber-reinforced composites is three-dimensional. For an embedded fiber of a finite radius, there are three options when a

DISCLAIMER

matrix crack reaches the interface: interface debonding, fiber fracture, or crack circumventing the fiber. The two-dimensional analysis [1] focuses on the case that the crack does not circumvent the fiber. However, when the crack circumvents the fiber, the crack is bridged by intact fibers, and the bridging-fiber (or fiber-pullout) geometry can be used to analyze this problem.

The purpose of the present study was to modify the two-dimensional bimaterial model [1] by considering two different geometries: (1) a strip of fiber sandwiched between two semi-infinite plates of matrix, and (2) a bridging-fiber geometry.

2. THE SANDWICH GEOMETRY

Schematic drawings of crack penetration and deflection for an oblique wedge-loaded crack used in the two-dimensional bimaterial model [1] are shown in Figs. 1 (a) and (b), respectively. Two semi-infinite elastic materials, material 1 and material 2, are bonded at the interface. The main crack in material 2 is subjected to opening wedge loads, P, at a distance, L, from the interface along the crack line. The crack intersects the interface at an oblique angle, ω_2, and can either penetrate the interface into material 1 or deflect at the interface. The branch crack has a length a. For the case of a penetrating crack (Fig. 1a), the angle between the branch crack and the interface is ω_1. To examine effects of a finite width of material 1, a layer of material 1 with a width, h, sandwiched between two semi-infinite material 2 was considered, and the schematic drawings for crack penetration and deflection are shown respectively in Figs. 1 (c) and (d).

For the plane-strain bimaterial problem, the solution variables of interest depend on two non-dimensional elastic mismatch parameters; i.e., the Dundurs' parameters [4] which are

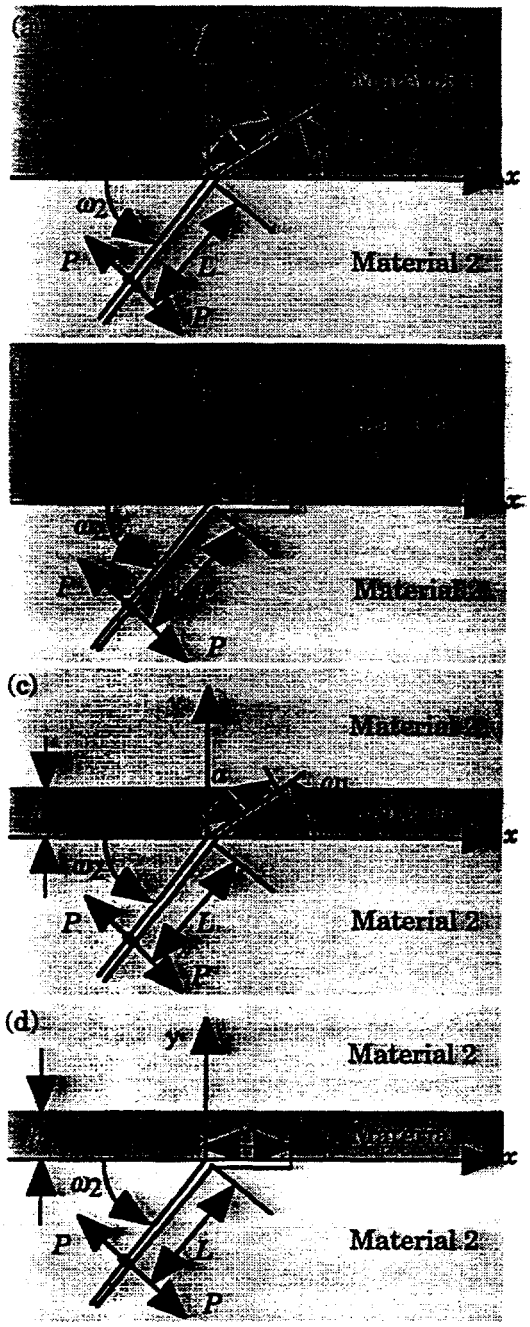

Figure. 1. Schematic drawings showing (a) a penetrating crack, and (b) a deflected crack for two semi-infinite dissimilar materials bonded at the interface, and (c) a penetrating crack, and (d) a deflected crack for material 1 with a width, h, sandwiched between two semi-infinite material 2.

$$\alpha = (\bar{E}_1 - \bar{E}_2)/(\bar{E}_1 + \bar{E}_2) \tag{1}$$

$$\beta = \frac{\mu_1(1-2\nu_2) - \mu_2(1-2\nu_1)}{2[\mu_1(1-\nu_2) + \mu_2(1-\nu_1)]} \tag{2}$$

where E, μ and ν are Young's modulus, shear modulus and Poisson's ratio, respectively, $\bar{E} = E/(1-\nu^2)$, and the subscripts 1 and 2 denote materials 1 and 2, respectively. Since experience with related problems suggests that α is the much more important one of the two parameters, the role of α is emphasized and β=0 is taken in the present study.

2.1. Analysis

Because of the complication of the problem, integral equation methods were not feasible, and a finite element method was used in the present study to analyze the energy release rates for a deflected crack and a penetrating crack.

The solutions for the stress intensity factors for the problem of a penetrating crack can be written as [1]

$$K_I + iK_{II} = c(\alpha, \omega_1, \omega_2, a/L)PL^{-1/2} \tag{3}$$

where c is a dimensionless complex-valued function of the arguments indicated. The corresponding energy release rate, G_p, is

$$G_p = \frac{(1-\nu_1)}{2\mu_1}|c|^2 \frac{P^2}{L} \tag{4}$$

It is noted that G_p is a function of ω_1, and the maximum value of G_p with respect to ω_1 for fixed a/L is denoted by G_p^{max}.

The stress intensity factors for a deflected crack can be expressed by [1]

$$K_1 + iK_2 = d(\alpha, \omega_2, a/L)PL^{-1/2} \tag{5}$$

where d is a dimensionless complex-valued function of the arguments indicated. The corresponding energy release rate of the deflected crack, G_d, is given by

$$G_d = \frac{1}{\bar{E}^*}|d|^2 P^2/L \tag{6}$$

where $\bar{E}^*$ is given by

$$\frac{1}{\bar{E}^*} = \left[\frac{1}{\bar{E}_1} + \frac{1}{\bar{E}_2}\right]\frac{1-\beta^2}{2} \equiv \frac{1-\beta^2}{(1-\alpha)\bar{E}_1} \tag{7}$$

The ratio of the competing energy release rates is hence

$$\frac{G_d}{G_p^{max}} = \frac{|d|^2}{(1-\alpha)|c|^2} \tag{8}$$

The numerical results presented in this paper were computed using a finite element code, ABAQUS [5], with eight node isoparametric elements. A quarter-point crack tip element served to model the inverse square root stress singularity at the crack tip. The detailed discussion about the numerical method can be found elsewhere [6], and the J-integral was calculated by the domain integral method [7] for ten contours to obtain strain energy release rates. The model employed in the finite element calculation was a circular region $r \le R$. In order to obtain the asymptotic solution, R should be much larger than both the length of the branch crack, a, and the distance from the wedge load to the crack tip, L. The convergence of the finite element solutions was examined, and it was found that the ratio R/L=1000 is sufficient to obtain the asymptotic solutions. Hence, $R/L \ge 1000$ was used in the present finite element analysis.

2.2. Results

The energy release rate ratio, G_d/G_p^{max}, as a function of α is plotted in Fig. 2 at

different widths of the sandwiched layer (i.e., material 1) for $\omega_2 = 30°, 45°, 60°$ and $75°$ and a/L=0.01 [8]. The curve for L/h=0 (i.e., $h \to \infty$) is also included which was the result presented in the earlier work [1]. The results in Fig. 2 show that the curve becomes flatter as the width of material 1 decreases (i.e., L/h increases).

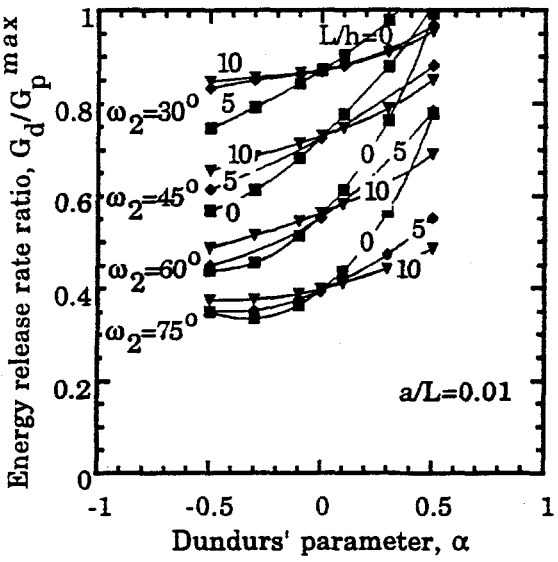

Figure. 2. The energy release rate ratio, G_d/G_p^{max}, as a function of the Dundurs' parameter, α, for a/L=0.01 at different values of L/h and ω_2.

3. A BRIDGING-FIBER GEOMETRY

When the crack circumvents the fiber, the crack surfaces are bridged by the intact fiber, and the applied tensile load is supported by the fiber. An idealized bridging-fiber (i.e., fiber-pullout) geometry [9] is shown in Fig. 3, in which one crack surface with the bridging fiber is shown. A fiber with a radius, a, is embedded in a coaxial cylindrical shell of matrix with a radius, b, and is subjected to a tensile stress in its axial direction.

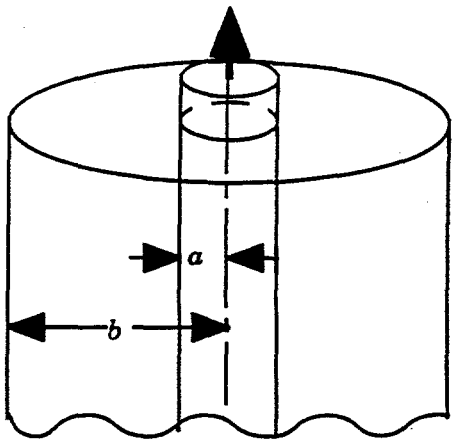

Figure. 3. A schematic drawing showing the bridging-fiber (i.e., pullout) geometry.

3.1. Analysis

Using the energy-based criterion, the relation between the tensile loading stress on the fiber to debond the interface, σ_d, and the interface debond energy, Γ_i, has been defined, such that [10,11]

$$\sigma_d = 2\left\{\frac{E_f \Gamma_i}{a}\left[\frac{b^2 E_c}{\left(b^2 - a^2\right)E_m}\right]\right\}^{1/2} \tag{9}$$

where

$$E_c = \frac{a^2 E_f + \left(b^2 - a^2\right)E_m}{b^2} \tag{10}$$

When σ_d is greater than the fiber strength, σ_s, fiber fracture occurs before interfacial debonding. However, construction of the diagram of interfacial debonding versus fiber fracture needs not only the interface debond energy, Γ_i, but also the fiber fracture energy, Γ_f [1]. To achieve this, the relation between σ_s and Γ_f is required which is derived as follows.

The relation between σ_s and Γ_f is a function of the shape and the size of the defect in the fiber. When the fiber has a small (compared to the fiber radius) defect of size c and is subjected to a tensile stress, σ, the stress intensity factor at the crack tip, K_I, can be expressed by a general equation, such that

$$K_I = \lambda\sigma\sqrt{\pi c} \qquad (11)$$

where λ is a defect-geometry factor (= 1.122 for a circumferential crack where c is the crack depth [12], = 0.637 for an internal penny-shaped crack where c is the crack radius [12], and = 0.34 for a thumb-nail flaw extending from the surface to the interior where c is the crack radius [13]). The corresponding strain energy release rate, G_f, is

$$G_f = \frac{\left(1-\nu_f^2\right)K_I^2}{E_f} \qquad (12)$$

Fiber fracture occurs when σ reaches σ_s and the corresponding G_f reaches Γ_f.

Combination of equations (11) and (12) gives

$$\sigma_s = \frac{1}{\lambda}\sqrt{\frac{E_f\Gamma_f}{\pi c\left(1-\nu_f^2\right)}} \qquad (13)$$

Substitution of equation (13) into equation (9) yields a critical ratio for Γ_i/Γ_f, such that

$$\left(\frac{\Gamma_i}{\Gamma_f}\right)_{crit} = \frac{a}{c\lambda^2}\frac{\left(b^2-a^2\right)E_m}{4\pi b^2\left(1-\nu_f^2\right)E_c} \qquad (14)$$

Interfacial debonding and fiber fracture occur when Γ_i/Γ_f is smaller and greater than the critical ratio, respectively.

3.2. Results

Using Eq. (14), the diagram of interfacial debonding versus fiber fracture is constructed in Fig. 4 [14], in which the Dundurs' parameter, α, is defined by Eq. (1), where the subscripts, 1 and 2, denote the fiber and the matrix, respectively.

It is noted that both the relative defect size, c/a, in the fiber and the defect-geometry factor, λ, are involved in defining the diagram. Interfacial debonding and fiber fracture occur when $c\lambda^2\Gamma_i/a\Gamma_f$ is below and above the curve, respectively, in Fig. 4. This critical ratio decreases with the increase in α. Also, the curve in Fig. 4 becomes flatter as b/a increases.

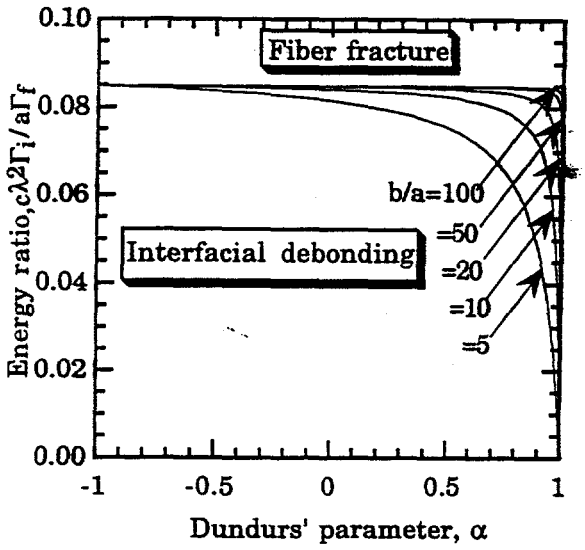

Fig. 4. The diagram of interfacial debonding versus fiber fracture for the bridging-fiber geometry.

4. CONCLUDING REMARKS

Considering a two-dimensional geometry, a diagram of interfacial debonding versus fiber fracture has been constructed previously based on the ratio of the interface debond energy to the fiber fracture energy, Γ_i/Γ_f [1]. The fiber and the

matrix are represented by two semi-infinite planes. Hence, when the matrix crack reaches the interface, it will either deflect into the interface or penetrate the fiber. One modification of this two-dimensional approach is to consider a finite width for the fiber, which is sandwiched between two semi-infinite planes of matrix. It was found that the critical ratio of Γ_i/Γ_f in defining the condition of interfacial debonding versus fiber fracture is a function of not only the Dundurs' parameter but also the fiber width. Specifically, the curve in the diagram of interfacial debonding versus fiber fracture becomes flatter when the fiber width decreases (Fig. 2).

Considering a bridging fiber behind the crack tip, the critical ratio of Γ_i/Γ_f was also derived in the present study. It was found that this critical ratio decreases with the increase in the Dundurs' parameter, α. Also, the curve in the diagram of interfacial debonding versus fiber fracture becomes flatter when the radius ratio of matrix to fiber, b/a, increases (Fig. 4). It is noted that the two-dimensional bimaterial model considers the case where the crack reaches the interface, and the crack either deflects along the interface or penetrates the fiber. The bridging-fiber model considers the case where the crack reaches the interface, circumvents the fiber leaving an intact bridging fiber, and is then followed by either interface debonding or fiber fracture.

Acknowledgments--The authors thank Drs. M. J. Lance and M. J. Andrews for reviewing the manuscript. Research sponsored by the U.S. Department of Energy, Division of Materials Sciences, Office of Basic Energy Sciences, under contract DE-AC05-96OR22464 with Lockheed Martin Energy Research Corp.

REFERENCES

1. M. Y. He and J. W. Hutchinson, Inter. J. Solids Structures, 25 (1989) 1053.
2. P. F. Becher, S. L. Hwang, and C. H. Hsueh, MRS Bulletin Series on Silicon-Based Ceramics, 20 (1995) 23.
3. E. Y. Sun, P. F. Becher, S. B. Waters, C. H. Hsueh, K. P. Plucknett, and M. J. Hoffmann, Ceramic Microstructures '96: Control at the Atomic Level, A. P. Tomsia and A. Glaeser (eds), Plenum Press, NY (1998) 779.
4. J. Dundurs, J. Appl. Mech., 36 (1969) 650.
5. ABAQUS Finite Element Code, Version 5.5, Hibbit, Karlsson and Sorensen, Inc., Pawtucket, RI.
6. M. Y. He, A. G. Evans, and J. W. Hutchinson, Inter. J. Solids Structures. 31 (1994) 3443.
7. C. F. Shih, B. Moran, and J. Nakamura, Int. J. Fracture, 30 (1986) 79.
8. M. Y. He, C. H. Hsueh, and P. F. Becher to be published.
9. C. H. Hsueh, Mater. Sci. Eng., A123 (1990) 1.
10. P. G. Charalambides and A. G. Evans, J. Am. Ceram. Soc., 72 (1989) 746.
11. C. H. Hsueh, Mater. Sci. and Eng., A159 (1992) 65.
12. H. Tada, P. C. Paris, and G. W. Irwin, The Stress Analysis of Cracks Handbook, Del Research Corporation, St. Louis, MO, 1973.
13. R. W. Rice, Treatise on Materials Science and Technology, Academic Press, New York, 11 (1978) 199.
14. C. H. Hsueh and P. F. Becher, Acta Mater., 46 (1998) 3237.